Identifying robustness in the regulation of foraging of ant colonies using an interaction based model with backward bifurcation

Oyita Udiani[1] , Noa Pinter-Wollman [2] and Yun Kang[3]

Abstract

Collective behaviors in social insect societies often emerge from simple local rules. However, only little is known about how these behaviors are dynamically regulated in response to environmental changes. Here, we use a compartmental modeling approach to identify factors that allow social insects to regulate collective foraging activity in response to their environment. We propose a set of differential equations describing the dynamics of: (1) available foragers inside the nest, (2) active foragers outside the nest, and (3) successful returning foragers, to understand how colony-specific parameters, such as baseline number of foragers, interactions among foragers, food discovery rates, successful forager return rates, and foraging duration might influence collective foraging dynamics, while maintaining functional robustness to perturbations. Our analysis indicates that the model can undergo a forward (transcritical) bifurcation or a backward bifurcation depending on colony-specific parameters. In the former case, foraging activity persists when the average number of recruits per successful returning forager is larger than one. In the latter case, the backward bifurcation creates a region of bi-stability in which the size and fate of foraging activity depends on the temporal distribution of the foraging workforce. We validate the model with experimental data from harvester ants (*Pogonomyrmex barbatus*) and perform sensitivity analysis. Our model provides insights on how simple, local interactions can achieve an emergent and fairly robust regulatory system of collective foraging activity in ant colonies.

Keywords: Foraging Dynamics; Social Insects; Transcritical Bifurcation; Backward Bifurcation; Bi-stability; Robustness

1. Introduction

The dynamics of collective foraging in social insects emerges from local feedback processes that couple the behavioral decisions of individual workers with the colony's intake requirements [1]. Because these systems are highly de-centralized, the foraging activity of a colony is not only dependent on how well information flow is regulated and distributed among foragers, but also on the robustness of these information channels to perturbations inside and outside the nest ([2, 3, 4]). Collective foraging of social insects has been extensively studied in many systems, revealing similarities in the dynamics of its regulation across species (e.g. Bees [5, 6]; Ants,[4, 7], etc). Although the individual components of these systems are highly nuanced, they share striking similarities in the temporal structure and non-linearity of information flow between active and inactive foragers.

Ant species exhibit a variety of foraging strategies that employ a combination of direct and indirect social cues [8]. Forager recruitment strategies range from leader-based recruitment in which successful foragers

[1]Mathematical, Computational and Modeling Sciences Center, Arizona State University, Tempe, 85287-1904 (Oyita.Udiani@asu.edu).

[2]BioCircuits Institute, University of California, San Diego, La Jolla CA. 92093-0328 USA (nmpinter@ucsd.edu).

[3]Sciences and Mathematics Faculty, School of Letters and Sciences, Arizona State University, Mesa, AZ 85212, USA (yun.kang@asu.edu).

guide recruits directly to the food source (i.e. tandem running; [9, 10]) to self-organizing pheromone trail networks that allow recruits to locate and exploit profitable food sources [11].

Mathematical models have been instrumental in uncovering some mechanisms that underlie the foraging dynamics of ant colonies when faced with changing environmental conditions ([6, 12, 13, 14]). For example, Beekman et al. [15] investigated the transition between disordered and ordered foraging as a function of colony size in Pharaoh's ants *Monomorium pharaonis*. Their model predicted a discontinuous phase transition between low foraging activity and high activity using pheromone trails when group size was intermediate and food sources were difficult to locate through independent searches. More recently, theoretical results from Collignon et al. [12] suggest that coupling leader-based recruitment with self-reinforcing pheromone trails may help *Tetramorium caespitum* colonies manage the costs of small group sizes and pheromone volatility on their foraging efficiency. Finally, Dussutour & Nicolis [16] explored the reliability of collective foraging decisions in a dynamic resource environment using chemical and non-chemical recruitment strategies in greenhead ants, *Rhytidoponera metallica*. Their analytical and empirical results suggest that interaction-based decision making (i.e. non-chemical recruitment) provides the colony with greater flexibility to track resource availability when food sources are ephemeral.

Although several models have addressed the dynamics of resource exploitation using pheromone-based forager recruitment (e.g.[6, 12, 14, 17]) few have considered systems without such spatial cues. This gap in the modeling literature is surprising because many species of ants forage independently either as scouts looking for new food sources, or as scavengers in a homogenous resource landscapes. The harvester ant *Pogonomyrmex barbatus* falls into this latter category. Colonies rely only on a very short chemical trail to determine daily forging direction [18]. However, the initiation and intensity of foraging activity is regulated by simple, brief interactions among workers [4, 19, 20, 21, 22]. Workers are more likely to leave the nest in search of seeds after reaching a threshold number of interactions with successful returning foragers in the area just inside the nest entrance called the ***vestibule*** [19, 23]. Forager return rate may serve as a reliable proxy for external foraging conditions (i.e. seed availability, humidity, etc.) because foragers are likely to continue their search until a seed item is found [24]. Antennal contacts are known to relay information among ants via cuticular hydrocarbons which can contain information about current and previously performed tasks [21, 25, 26]. Furthermore, these hydrocarbons combined with seed odors can convey information about food availability and influence foraging decisions of recently contacted workers [23]. Overall, these studies indicate that interactions among workers in the vestibule are fundamental for regulating patterns of foraging activity.

A recent study of the harvester ant *P. barbatus* by Pinter-Wollman *et al.* [19] not only quantifies the impacts of external perturbations on foraging dynamics but also raises interesting questions about the potential effects of colony-specific traits associated with forager behavior and other nested factors that may influence a colony's ability to regulate foraging activity. These traits may readily modulate the dynamics of forager availability within the vestibule. For instance, Pinter-Wollman *et al.* [19] reported that the threshold number of effective contacts necessary for forager activation varied among colonies even when forager return rates were similarly high. Likewise, colonies showed variation in their baseline number of available foragers and their ability to recover after a perturbation [19, 29].

To date, only few models have attempted to investigate the dynamics of physical interactions on collective activity [16, 30, 31]. An exception to this is a recent work by Prabhakar *et al.* [32] in which the authors developed a simple stochastic recursive algorithm inspired by the foraging ecology of *P. barbatus*. Approximating the inter-arrival times of successive returning foragers as a Poisson process, they generated a simple linear relation between the rates of incoming foragers and outgoing foragers assuming that each returning forager increased the rate of outgoing foragers by a fixed amount. Although their model captured many aspects of the data, including previously reported correlations between returning and outgoing foragers during periods of high food availability [19, 33, 34], the authors conceded some limitations. In short, their model could neither account for the non-linear patterns of forager interaction, nor mechanistically define parameters, which influence the rate of incoming foragers and their effects on inactive foragers in the nest.

In this paper, we develop a set of non-linear differential equations which focuses on the mechanistic pro-

cess of forager recruitment and accounts for the non-linearities of forager interaction in line with a previously described framework [13]. Our model captures the interaction-based regulation of foraging activity in ant colonies by delineating the foraging workforce into three categories: (1) available foragers at the nest, (2) active foragers outside the nest, and (3) successful returning foragers. These three components correspond to the classifications used in the recent work of *P. barbatus* [19]. This modeling approach will allow us to: (a) understand how external foraging variables and internal colony-specific parameters combine to influence the strength of forager recruitment and patterns of activity and (2) identify important parameters that may help improve the robustness of colony activity to perturbations.

In summary, we present a simple, generalizable model describing the interaction-based regulation of collective activity in social insects. Our model applies to foraging ecology of harvester ant colonies, but the framework remains applicable to analogous systems that rely on local worker interactions (e.g. nest construction in social wasps [35], quorum-sensing in rock ants, [36], etc). We investigate how the foraging activity of harvester ant colonies is influenced by forager recruitment rates as well as how the dynamics of worker availability can impact this relationship. In addition, we quantify the relative effects of colony-specific parameters (e.g. waiting times in the vestibule) by performing a sensitivity analysis based on the experimental data in [19].

The rest of the paper is structured as follows: In section 2, we motivate and develop our foraging model with general parameters. In section 3, we summarize the complete mathematical analysis of its dynamics and provide relevant biological implications. In section 4, we validate the model by comparing simulations with the empirical findings of [19], and present results on sensitivity analysis. We conclude with a biological discussion of our results and some closing remarks in section 5. Analytical details and proofs of our main results are presented in section 6.

2. Model Derivations

We develop a compartmental model of foraging activity (Fig. 1) inline with a general framework outlined in [13]. The model's state variables are defined as follows: let $N(t) = A(t) + F(t) + R(t)$ denote the total forager workforce of a focal colony at time t; where: $A(t)$ denotes the number of available foragers inside the nest (vestibule), $F(t)$ denotes the number of outgoing (activated) foragers on the trail, and $R(t)$ denotes the number of successful returning foragers on the foraging trail. We focus our model on the foraging dynamics of a mature colony over the course of hourly activity [37]. Further, we make the following assumptions about the colony's behavioral and foraging ecology:

1. **Available Foragers A:** The numbers of available foragers $A(t)$ is determined by four flow rates:

   The inflow rate consists of two components:

   (a) The ***arrival rate*** $\Lambda(t)$ which describes the movement of available foragers from the inner nest to the vestibule. This rate may vary over the course of daily activity depending on the colony's state and other life history properties such as the number of workers allocated to foraging tasks, colony age, etc. ([37, 38]). We assume that $\Lambda(t) = k_1$ is approximately constant over our timescale of interest.

   (b) The ***per-capita return rate*** γ at which returning foragers become re-available for recruitment. This rate will be influenced by the distance between the resource site and the nest; the time spent searching for seeds, the average traveling speed, and the time spent inside the nest after a foraging trip (e.g. depositing seed caches). We aggregate these delays into a single constant $(1/\gamma)$ which describes the average time spent as a returning forager.

   The outflow rate consists of two components:

(a) The ***activation rate*** of available foragers βAR which increases the number of active foragers on the trail. This formulation assumes mass action incidence and is supported by the experimental results of [19, 21]. More specifically, we assume that: (i) at any time, available foragers interact with a fraction ρ of returning foragers in the vestibule at the per-capita rate c, and (ii) interactions are independent and equally likely to occur between available and returning foragers. Hence, the effective contact rate (β) is the product of the number of interactions per unit time made by a returning forager and the probability (μ) that an interaction activates a new forager (i.e. $\beta = c\rho\mu$).

(b) The ***retirement rate*** of available foragers from the vestibule into the inner nest k_2 which is discounted by the factor: $\frac{A}{1+R}$. This formulation reflects the adaptive behavior of available foragers in response to changes in forager return rate reported in [19]. If the number of available foragers is large relative to the number of returning foragers, the vestibule becomes crowded and available foragers are more likely to retire to the inner nest at a maximum rate k_2 (when there are no returning foragers: $R = 0$). On the other hand, if R is large (implying resource abundance) then available foragers are less likely to retire into the inner nest.

Based on these assumptions, we formulate the dynamics of the available foragers as follows:

$$A' = \underbrace{k_1}_{\text{arrive}} + \underbrace{\gamma R}_{\text{return}} - \underbrace{\beta AR}_{\text{activate}} - \underbrace{k_2 \frac{A}{1+R}}_{\text{retire}} \tag{1}$$

2. **Active Foragers** F**:** The number of active foragers $F(t)$ on the trail is determined by the forager activation rate βAR; the rate of resource discovery, $\alpha(S)F$; and the loss (or death) rate $d_f F$ while searching for the resource (e.g. due to predatory activity near foraging trails [27]). The rate $\alpha(S)F$ at which active foragers F become returning foragers R is influenced by the abundance of available food resource, S. For mature harvester ant colonies, the effective seed densities around the nest's home range are typically orders of magnitude greater than the maximum number of foragers [33]. Thus, seed abundance should be generally (approximately) independent of a colony's foraging intensity especially on the timescale of daily activity. Hence, we will assume that the resource capture rate is constant within a day: $\alpha(S) = \alpha$. We also assume foragers continue to search until they encounter a food item as is typical for seed harvester ants [24]. Based on these ecological assumptions, we formulate the dynamics of the active foragers as follows:

$$F' = \underbrace{\beta AR}_{\text{activate}} - \underbrace{\alpha F}_{\text{discover food}} - \underbrace{d_f F}_{\text{dead/lost}} \tag{2}$$

3. **Returning foragers** R**:** The number of returning foragers $R(t)$ on the trail is determined by the rate at which active foragers discover food items, αF; the rate at which foragers return to the nest and become re-available for recruitment γR; as well as the rate of predation and/or loss while en-route to the nest $d_r R$. Based on these assumptions, we formulate the dynamics of the returning foragers as follows:

$$R' = \underbrace{\alpha F}_{\text{discover food}} - \underbrace{\gamma R}_{\text{return}} - \underbrace{d_r R}_{\text{dead/lost}} \tag{3}$$

Thus, the model is formulated as the following system of ordinary differential equations:

$$\begin{aligned} A' &= k_1 + (\gamma - \beta A)R - k_2 \tfrac{A}{1+R} \\ F' &= \beta AR - (\alpha + d_f)F \\ R' &= \alpha F - (\gamma + d_r)R \end{aligned} \tag{4}$$

hereafter referred to as foraging model (4).

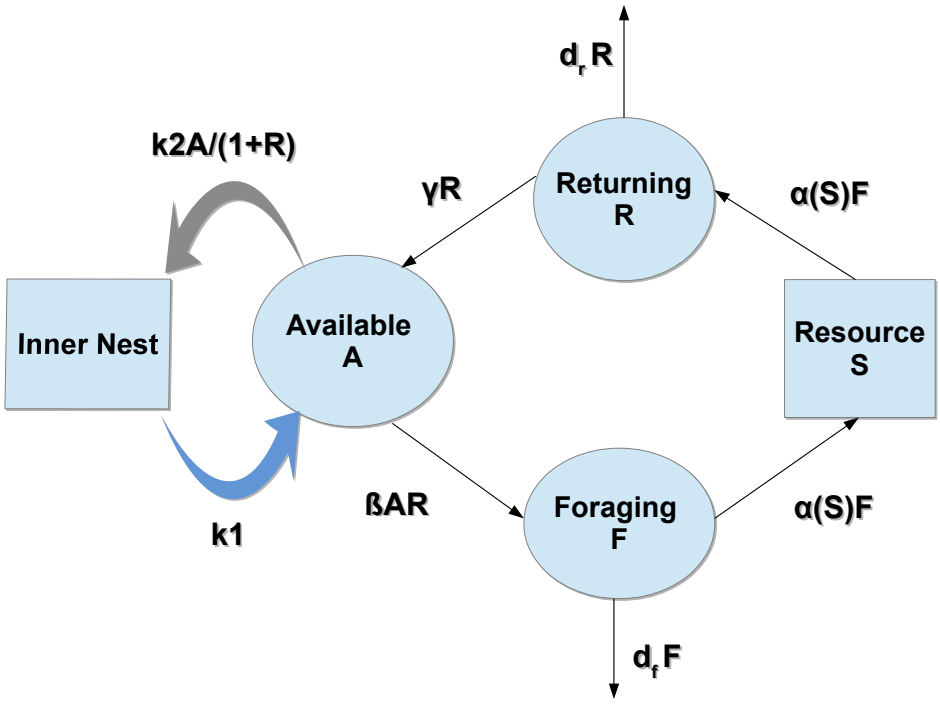

Figure 1: Flow diagram of the proposed foraging model (4). The dynamics of the rectangular components (i.e. *Inner Nest & Resource S*, assumed to be independent of the foraging activity on our time-scale of interest. Parameters definitions are given in Table 1.

3. Mathematical Analysis

We first provide the basic dynamic properties of the foraging model (4) in the following theorem:

Theorem 3.1. *[Compact Attractor] The foraging model (4) is positively invariant in $\mathbb{R}^3_+$ and every trajectory starting in $\mathbb{R}^3_+$ is attracted to the following compact set C:*

$$C = \left\{ (A, F, R) \in \mathbb{R}^3_+ : \frac{k_1}{\max\{k_2, d_f, d_r\}} \leq A + F + R \leq \frac{k_1 + \frac{k_1^2}{4d_r}}{\min\{k_2, d_f, d_r\}} \right\}. \tag{5}$$

In addition, the number of available foragers A is persistent.

Notes: Theorem 3.1 implies that our foraging model (4) is well defined (i.e. biologically plausible) because the total foraging workforce (N) is bounded, and all compartments remain nonnegative for nonnegative initial conditions.

Parameter	Description	Range	Baseline	Source
k_1	Arrival rate ($ants \cdot sec^{-1}$)	$(0, 5)$	1	Assumption
k_2	Retirement rate ($ants \cdot sec^{-1}$)	$(0, 5)$	0.25	Assumption
β	Effective contact rate ($ants \cdot sec^{-1}$)	$(0, 1)$	0.1	[19]
γ	Per-capita forager return rate (sec^{-1})	$(0, 5)$	0.01	[4, 19]
α	Resource discovery rate ($seeds \cdot sec^{-1}$)	(0,1)	1	[28, 33, 39]
d_f	Loss rate: outbound foragers (sec^{-1})	$(0, 10)$	0.05	Assumption
d_r	Loss rate: inbound foragers (sec^{-1})	$(0, 10)$	0.05	Assumption

Table 1: Parameter definitions used in model (4). Sampling ranges were compiled (or estimated) from cited sources. Baseline parameter values were used for parameter estimation and sensitivity analysis in section 4.

3.1. Equilibria and their stability

An equilibrium of the foraging model (4) should satisfy the following equations:

$$\begin{aligned} R' &= \alpha F - (\gamma + d_r)R = 0 \Leftrightarrow F = \tfrac{\gamma+d_r}{\alpha}R \\ F' &= \beta AR - (\alpha + d_f)F = 0 \Leftrightarrow A = \tfrac{(\alpha+d_f)F}{\beta R} = \tfrac{(\alpha+d_f)\frac{\gamma+d_r}{\alpha}R}{\beta R} = \tfrac{(\alpha+d_f)(\gamma+d_r)}{\alpha\beta} \\ A' + F' + R' &= k_1 - k_2\tfrac{A}{1+R} - d_f F - d_r R = 0 \Leftrightarrow k_1 - k_2\tfrac{A}{1+R} - \tfrac{d_f(\gamma+d_r)}{\alpha}R - d_r R = 0. \end{aligned} \tag{6}$$

Thus, we have the following two cases:

1. When $F = R = 0$, model (4) has a unique **non-foraging equilibrium**: $\mathscr{E}_{\mathbf{0}} = (A_0^*, 0, 0) = (\frac{k_1}{k_2}, 0, 0)$. This equilibrium always exits. Note that $A_0^* = \frac{k_1}{k_2}$ defines a *baseline number of available foragers* in the vestibule in the absence of returning foragers, and is determined by the ratio of worker arrival to forager retirement rates.

2. When $F \neq 0, R \neq 0$, model (4) has at most two **foraging equilibria**: $\mathscr{E}_i = (A_f^*, F_i^*, R_i^*) = \left(A_f^*, \frac{\gamma+d_r}{\alpha}R_i^*, R_i^*\right)$ $i = 1, 2$ where;

$$A_f^* = \frac{(\alpha + d_f)(\gamma + d_r)}{\alpha\beta} > \frac{\gamma}{\beta} \Rightarrow \beta A_f^* - \gamma > 0 \tag{7}$$

and R_i^* are the roots of the equation $\phi(R^*) = k_2 A_f^*$ because:

$$k_1 - k_2\tfrac{A_f^*}{1+R^*} - \tfrac{d_f(\gamma+d_r)}{\alpha}R^* - d_r R^* = \tfrac{\left[k_1 - \frac{d_f(\gamma+d_r)+d_r\alpha}{\alpha}R^*\right](1+R^*) - k_2 A_f^*}{1+R^*} = \tfrac{\phi(R^*) - k_2 A_f^*}{1+R^*} = 0.$$

Notice that when $\frac{d_f(\gamma+d_r)+d_r\alpha}{\alpha} = \beta A_f^* - \gamma > 0$, we have the following equalities

$$\phi(R^*) = \left[k_1 - \frac{d_f(\gamma + d_r) + d_r\alpha}{\alpha}R^*\right](1 + R^*) = \left[k_1 - (\beta A_f^* - \gamma)R^*\right](1 + R^*). \tag{8}$$

Moreover, we are able to solve R_i^* explicitly as follows:

$$R_{1,2}^* = \frac{(\gamma - \beta A_f^* + k_1) \pm \sqrt{(\gamma - \beta A_f^* + k_1)^2 + 4(\beta A_f^* - \gamma)(k_1 - k_2 A_f^*)}}{2(\beta A_f^* - \gamma)}, \qquad R_1^* < R_2^*. \tag{9}$$

To continue our analysis, we make the following observations and define quantities which largely determine the dynamics of Model (4):

1. First, notice that the equation $\phi(R) = \left[k_1 - (\beta A_f^* - \gamma)R\right](1+R)$ has a unique maximum ϕ_{max} at its critical point $R_c = \frac{\gamma - \beta A_f^* + k_1}{2(\beta A_f^* - \gamma)} = \frac{\alpha(k_1 - d_r) - d_f(\gamma + d_r)}{2[\alpha d_r + d_f(\gamma + d_r)]}$. Thus we define:

$$\phi_{max} = \phi(R_c) = \frac{(\beta A_f^* - \gamma + k_1)^2}{4(\beta A_f^* - \gamma)} = \frac{[\alpha(k_1 - d_r) - d_f(\gamma + d_r)]^2}{4\alpha[\alpha d_r + d_f(\gamma + d_r)]} \geq \phi(0) = k_1 \tag{10}$$

2. We define $\mathcal{R}_0$ as the ***forager generation number*** where

$$\mathcal{R}_0 \quad = \quad \frac{A_0^*}{A_f^*} = \frac{k_1/k_2}{\frac{(\alpha + d_f)(\gamma + d_r)}{\alpha\beta}} = \frac{k_1}{k_2}\frac{\alpha\beta}{(\alpha + d_f)(\gamma + d_r)}. \tag{11}$$

   $\mathcal{R}_0$ estimates the expected number of new foragers generated by the return of a successful forager when foraging levels are close to the no-activity steady-state. This is applicable, for instance, at the commencement of morning activity when trail patrollers are returning to the nest or after a large foraging interruption [4]. Notice that $\mathcal{R}_0$ is dimensionless because:

$$\mathcal{R}_0 = \frac{A_0^*}{A_f^*} = \underbrace{\frac{k_1}{k_2}}_{\text{Baseline available foragers}} \cdot \underbrace{\alpha}_{\text{Resource discovery rate}} \cdot \underbrace{\beta}_{\text{Contact rate}} \cdot \underbrace{\frac{1}{(\gamma + d_r)(\alpha + d_f)}}_{\text{Mean foraging duration}}$$

   where $A_0^* = \frac{k_1}{k_2}$ is the baseline number of available foragers in the vestibule, and $\tau = \frac{1}{(\gamma + d_r)(\alpha + d_f)}$ is the average duration of a foraging trip. Intuitively, we expect that colonies will maintain foraging activity if each returning forager activates more than one new forager (i.e. $\mathcal{R}_0 > 1$).

3. Model (4) can undergo a ***backward bifurcation*** as our analysis reveals later in this section. This bifurcation is characterized by the emergence of a second threshold:

$$\mathcal{R}_\Delta \quad = \quad \frac{\phi(0)}{\phi_{max}} = \frac{k_1}{\phi_{max}} = \frac{4k_1(\beta A_f^* - \gamma)}{(\beta A_f^* - \gamma + k_1)^2} = \frac{4k_1\alpha[\alpha d_r + d_f(\gamma + d_r)]}{[\alpha(k_1 - d_r) - d_f(\gamma + d_r)]^2} \leq 1 \tag{12}$$

   As discussed in section 6, mathematically $\mathcal{R}_\Delta$ represents a sub-critical threshold value when Model (4) goes from having zero to two interior equilibria (Fig. 3(b)). Biologically, however, it defines a lower bound for $\mathcal{R}_0$ (i.e. the minimum number of new forager recruits that are necessary for maintaining foraging activity).

The stability of an equilibrium $E^* = (A^*, F^*, R^*)$ is determined by the Jacobian matrix (13) of Model (4) evaluated at the equilibrium:

$$J|_{E^* = (A^*, F^*, R^*)} := \begin{bmatrix} -\beta R^* - \frac{k_2}{1+R^*} & 0 & -\beta A^* + \gamma + \frac{k_2 A^*}{(1+R^*)^2} \\ \beta R^* & -(\alpha + d_f) & \beta A^* \\ 0 & \alpha & -(\gamma + d_r) \end{bmatrix}. \tag{13}$$

The following theorem provides the explicit condition on the existence and local stability of the **non-foraging equilibrium** $\mathscr{E}_\mathbf{0}$ and the **foraging equilibrium** $\mathscr{E}_i, i = 1, 2$.

Theorem 3.2 (Existence & Stability of Equilibria)**.** *The foraging model (4) can have one ($\mathscr{E}_\mathbf{0}$), two ($\mathscr{E}_\mathbf{0}$ and $\mathscr{E}_\mathbf{2}$), or three equilibria ($\mathscr{E}_\mathbf{0}$ and $\mathscr{E}_\mathbf{i}, i = 1, 2$) depending on the values of $\mathcal{R}_0$ and $\mathcal{R}_\Delta$. Sufficient conditions for the existence and local stability of these equilibria are summarized in Table (2).*

Equilibria	Existence Condition	Stability Condition
$\mathscr{E}_{\mathbf{0}}$	Always	Locally stable if $\mathcal{R}_0 < 1$ but a saddle if $\mathcal{R}_0 > 1$
$\mathscr{E}_{\mathbf{1}}$	$\max\{\frac{k_1\beta}{k_2(k_1+\gamma)}, \mathcal{R}_\Delta\} < \mathcal{R}_0 < 1$	Always a saddle
$\mathscr{E}_{\mathbf{2}}$	$\mathcal{R}_0 > \max\{\frac{k_1\beta}{k_2(k_1+\gamma)}, \mathcal{R}_\Delta\}$ or $1 < \mathcal{R}_0 < \frac{k_1\beta}{k_2(k_1+\gamma)}$	Always locally stable

Table 2: Equilibria and their stability where $\mathcal{R}_0 = \frac{k_1}{k_2 A_f^*}$, $\mathcal{R}_\Delta = \frac{k_1}{\phi_{max}}, \phi_{max} = \frac{(\beta A_f^* - \gamma + k_1)^2}{4(\beta A_f^* - \gamma)}$ and $A_f^* = \frac{(\alpha+d_f)(\gamma+d_r)}{\alpha\beta}$.

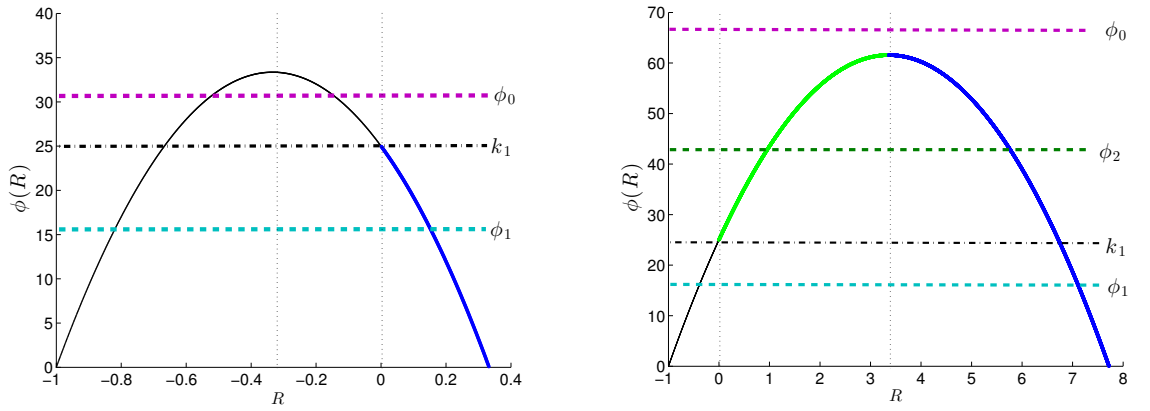

(a) $R_0 > 1$: only $\mathscr{E}_0$ or ($\mathscr{E}_0$ & $\mathscr{E}_2$)

(b) $\max\{\frac{k_1\beta}{k_2(k_1+\gamma)}, \mathcal{R}_\Delta\} < \mathcal{R}_0 < 1$: only $\mathscr{E}_0$ or $(\mathscr{E}_i, i = 0, 2)$ or $(\mathscr{E}_i, i = 0, 1, 2)$

Figure 2: Schematic nullclines of the foraging model (4). Biologically feasible (i.e positive) equilibria occur at intersections between $\phi(R)$ and the dashed horizontal lines (ϕ_i , $i = 1, 2$) where $\phi_i < k_1$. Equilibrium points on $\phi(R)$ are classified as attractors (blue), saddles (green) or repellers (black). There are no positive equilibria on the line ϕ_0. Otherwise, model (4) either has a unique foraging equilibrium (ϕ_1, left panel) or two (ϕ_2, right panel).

Notes: Theorem 3.2 implies that: (i) the values of $\mathcal{R}_0$ and $\mathcal{R}_\Delta$ determine the existence of the foraging equilibrium $\mathscr{E}_{\mathbf{i}}, i = 1, 2$ (see Table 2 and Fig. 2); (ii) the foraging model (4) only exhibits equilibrium behavior (i.e. there are no periodic or chaotic dynamics); and (iii) the **non-foraging equilibrium** $\mathscr{E}_{\mathbf{0}} = (A_0^*, 0, 0) = (\frac{k_1}{k_2}, 0, 0)$ and the **foraging equilibrium** $\mathscr{E}_2 = (A_f^*, F_2^*, R_2^*) = \left(A_f^*, \frac{\gamma+d_r}{\alpha}R_2^*, R_2^*\right)$ are both locally asymptotically stable whenever $\max\{\frac{k_1\beta}{k_2(k_1+\gamma)}, \mathcal{R}_\Delta\} < \mathcal{R}_0 < 1$ (see Fig. 2(b)-3(b)).

3.2. Global dynamics: Backward bifurcation

Based on our analytical results shown in Theorem 3.1-3.2, we can classify global dynamics of the foraging model (4) in terms of $\mathcal{R}_0$ and $\mathcal{R}_\Delta$ as the following theorem:

Corollary 3.1 (Global Dynamics)**.** *Depending on the values of $\mathcal{R}_0$ and $\mathcal{R}_\Delta$, the global dynamics of the foraging model (4) can be classified into one of three scenarios (also see Table 3):*

1. ***No foraging activity:*** *If $\mathcal{R}_0 < \min\{1, \frac{k_1\beta}{k_2(k_1+\gamma)}\}$ or $\frac{k_1\beta}{k_2(k_1+\gamma)} < \mathcal{R}_0 < \mathcal{R}_\Delta$, then the foraging model (4) has only* the non-foraging equilibrium $\mathscr{E}_{\mathbf{0}} = (\frac{k_1}{k_2}, 0, 0)$ *which is globally stable.*

2. ***Persistent foraging activity:*** *If $\mathcal{R}_0 > 1$, then the foraging model (4) has* the non-foraging equilibrium $\mathscr{E}_{\mathbf{0}}$ *and* the foraging equilibrium $\mathscr{E}_{\mathbf{2}}$ *where $\mathscr{E}_{\mathbf{0}}$ is a saddle and $\mathscr{E}_{\mathbf{2}}$ is globally stable.*

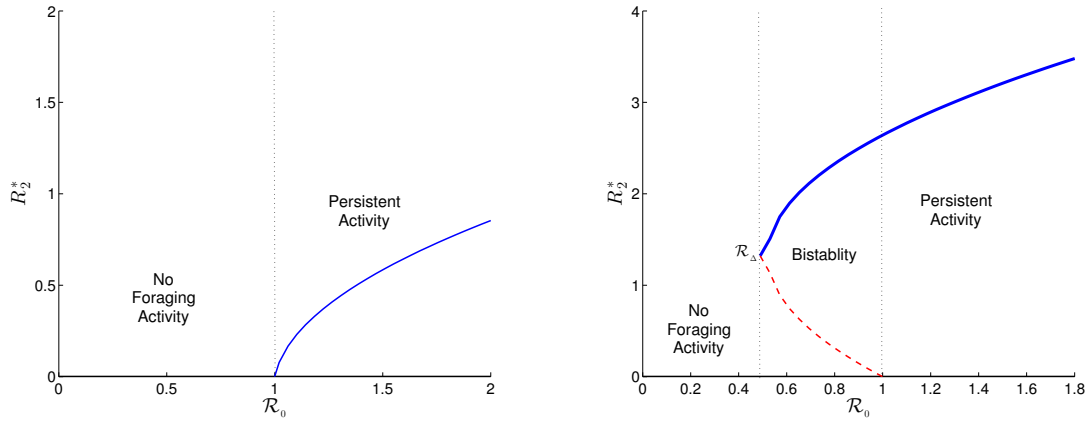

(a) (b)

Figure 3: One-dimensional bifurcation diagrams of model (4) for (a) $R_0 > 1$ and (b) $\max\{\frac{k_1\beta}{k_2(k_1+\gamma)}, \mathcal{R}_\Delta\} < \mathcal{R}_0 < 1$. The origin ($R_2^* = 0$) corresponds to the non-foraging equilibrium state which is stable whenever $\mathcal{R}_0 < 1$, and unstable otherwise. A stable interior equilibrium (blue) bifurcates "forward" from the origin when $\mathcal{R}_0 = 1$ (left panel). An unstable interior equilibrium (red) bifurcates"backward" from the origin when $\mathcal{R}_0 = 1$ and merges with its stable branch at $\mathcal{R}_\Delta$.

3. ***Bi-stablity:*** *If* $\max\{\frac{k_1\beta}{k_2(k_1+\gamma)}, \mathcal{R}_\Delta\} < \mathcal{R}_0 < 1$, *then the foraging model* (4) *has* the non-foraging equilibrium $\mathscr{E}_\mathbf{0}$ *and* two foraging equilibria $\mathscr{E}_\mathbf{i}, i = 1, 2$ *where both* $\mathscr{E}_\mathbf{0}$ *and* $\mathscr{E}_\mathbf{2}$ *are locally asymptotically stable.*

Equilibria	Existence Condition	Dynamics
Only $\mathscr{E}_\mathbf{0}$	$\mathcal{R}_0 < \min\{1, \frac{k_1\beta}{k_2(k_1+\gamma)}\}$ or $\frac{k_1\beta}{k_2(k_1+\gamma)} < \mathcal{R}_0 < \mathcal{R}_\Delta$	Globally stable.
$\mathscr{E}_\mathbf{0}$ and $\mathscr{E}_\mathbf{2}$	$\mathcal{R}_0 > 1$	$\mathscr{E}_\mathbf{0}$ is a saddle and $\mathscr{E}_\mathbf{2}$ is globally stable
$\mathscr{E}_\mathbf{i}, i = 0, 1, 2$	$\max\{\frac{k_1\beta}{k_2(k_1+\gamma)}, \mathcal{R}_\Delta\} < \mathcal{R}_0 < 1$	Both $\mathscr{E}_\mathbf{0}$ and $\mathscr{E}_\mathbf{2}$ are locally stable and $\mathscr{E}_\mathbf{1}$ is a saddle.

Table 3: Equilibria and their stability where $\mathcal{R}_0 = \frac{k_1}{k_2 A_f^*}$, $\mathcal{R}_\Delta = \frac{k_1}{\phi_{max}}$, $\phi_{max} = \frac{(\beta A_f^* - \gamma + k_1)^2}{4(\beta A_f^* - \gamma)}$ and $A_f^* = \frac{(\alpha + d_f)(\gamma + d_r)}{\alpha\beta}$.

Notes: According to our analytical results Theorem 3.1-3.2 and their corollary 3.1, we conclude that the foraging model (4) exhibits two kinds of global dynamics (see Fig. 3).

1. If $R_0 > 1$, Model (4) undergoes a forward (transcritical) bifurcation at $\mathcal{R}_0 = 1$ characterized by the emergence of a globally stable *foraging activity equilibrium* $\mathscr{E}_\mathbf{2}$ (see Fig. 3(a)).
2. If $\max\{\frac{k_1\beta}{k_2(k_1+\gamma)}, \mathcal{R}_\Delta\} < \mathcal{R}_0 < 1$, Model (4) undergoes a backward (sub-critical) bifurcation as $\mathcal{R}_0$ decreases past $\mathcal{R}_0 = 1$ and a saddle-node bifurcation at $\mathcal{R}_0 = \mathcal{R}_\Delta$. The backward bifurcation creates a region of bi-stability within $\max\{\frac{k_1\beta}{k_2(k_1+\gamma)}, \mathcal{R}_\Delta\} < \mathcal{R}_0 < 1$ (see Fig. 3(b)).

Biological Implications: Our analytical results show that the ***forager generation number*** ($\mathcal{R}_0$) and its sub-critical threshold ($\mathcal{R}_\Delta$) play essential roles in the foraging dynamics of Model (4). $\mathcal{R}_0$ is influenced by a combination of internal and external variables including forager interaction rates in the vestibule (β),

local resource densities (α), and the average duration of foraging trips ($\frac{1}{(\gamma+d_r)(\alpha+d_f)}$). This result goes significantly further than previous models (e.g [29, 32]) in describing some underlying factors that can influence the effects of forager return rates on the recruitment of new foragers.

Moreover, because the baseline numbers of available foragers A_0^* is determined by the colony-specific activity levels which determine the rates at which workers arrive (k_1) and retire (k_2) from the vestibule, we suggest that $\mathcal{R}_0$ may be regulated by the colony, at least partially. We note also that:

1. When $\mathcal{R}_0$ is greater than 1, then foraging activity is **persistent**.
2. When $\mathcal{R}_0$ is small, such that $\mathcal{R}_0 < \min\{1, \frac{k_1\beta}{k_2(k_1+\gamma)}\}$ or $\frac{k_1\beta}{k_2(k_1+\gamma)} < \mathcal{R}_0 < \mathcal{R}_\Delta$, then the colony has **no foraging activity**.
3. When $\mathcal{R}_0$ is in the intermediate range, i.e., $\max\{\frac{k_1\beta}{k_2(k_1+\gamma)}, \mathcal{R}_\Delta\} < \mathcal{R}_0 < 1$, then the colony may or may not forage, depending on the size of the forager workforce and distribution between available A, activated F, and returning foragers R. In this case, the system is **bi-stable**.

Therefore, colonies can enter an inactive (non-foraging) state if per-capita numbers of new forager recruitment are reduced due to either: (1) external pressures on forager return rates (e.g., increased forager predation); or (2) internal pressures on forager availability (e.g., changes in colony task allocation that decrease the rate of worker arrivals to the vestibule from inside the nest). On the other hand, starting from low levels of activity, colonies can abruptly achieve high foraging returns when each forager recruits at least one available ant from the vestibule ($\mathcal{R}_0 > 1$). Subsequent reductions in $\mathcal{R}_0$ below one may not necessarily lead to foraging inactivity. This hysteretic effect of $\mathcal{R}_0$ is discussed in the next subsection.

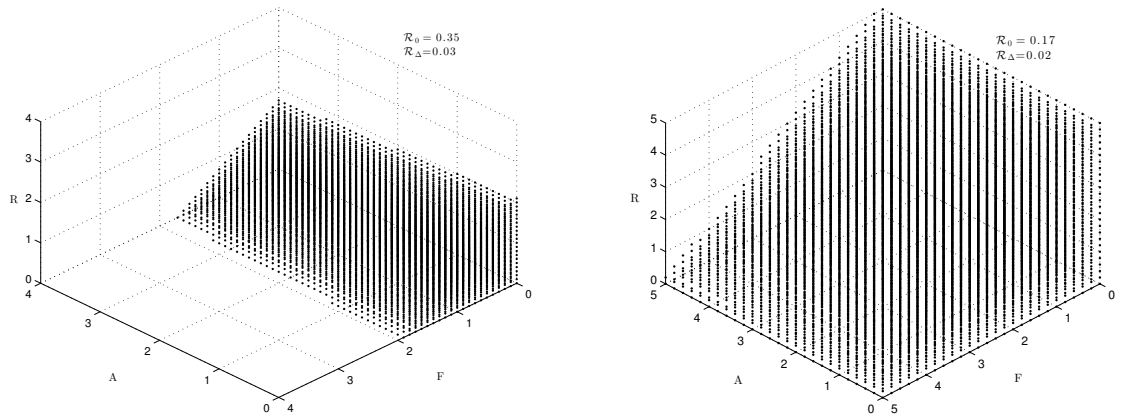

(a) $\beta = .005$ (b) $\beta = .0025$

Figure 4: Basin of attraction for the *non-foraging equilibrium*, $\mathscr{E}_0$ for high (a) and low (b) values of β, the effective contact rate. For fixed A, the basin has a negative slope in the $R-F$ plane suggesting that the numbers of returning foragers required to sustain activity is inversely proportional to the number of active foragers. Other parameters: $k_1 = 0.5$, $k_2 = 0.2$, $\gamma = .033$, $\alpha = 0.2$, $d_f = 2d_r = .005$.

3.3. Bi-stability and Foraging Robustness

The foraging model (4) is bi-stable whenever $\max\{\frac{k_1\beta}{k_2(k_1+\gamma)}, \mathcal{R}_\Delta\} < \mathcal{R}_0 < 1$. In this case, a critical distribution of the forager workforce defines a basin of attraction for $\mathscr{E}_\mathbf{0}$ and $\mathscr{E}_\mathbf{2}$. Fig. 4 provides two such

examples indicating the influence of the effective contact rate (β) on the basin of attraction for the *non-foraging equilibrium*. Now, let ξ denote the difference between the forager generation number $\mathcal{R}_0$ and $\mathcal{R}_\Delta$; that is:

$$\xi = \mathcal{R}_0 - \mathcal{R}_\Delta = \frac{k_1}{k_2 A^*} \cdot \left(\frac{\phi_{\max} - k_2 A^*}{\phi_{\max}} \right) = \frac{k_1}{k_2 A^*} \cdot \left(1 - \frac{4(\beta A^* - \gamma) k_2 A^*}{(\beta A^* - \gamma + k_1)^2} \right) \tag{14}$$

Biologically, we suggest that ξ defines a simple robustness metric potentially useful for evaluating inter-colony differences in foraging intensity under favorable environmental conditions. We make this suggestion because the magnitude of ξ correlates with the size of the basin of attraction for the colony's non-foraging state ($\mathscr{E}_{\mathbf{0}}$). First, note that model (4) is bi-stable whenever $\xi = \mathcal{R}_0 - \mathcal{R}_\Delta > 0$ holds. Colonies with larger values of ξ would have a larger region of bi-stability below $\mathcal{R}_0 < 1$ and thus have greater robustness to perturbations that further reduce the rate of returning foragers. This observation is in accordance with previous empirical studies which report that colonies show variation in their responsiveness and reduction of foraging activity under sustained disruptions to forager return rates [4, 34, 29].

From a modeling standpoint, it is of interest to understand what kinds of parameter changes could affect the robustness of foraging activity. We have distinguished between internal foraging parameters that likely depend on colony-specific traits (i.e. k_1, k_2, β, & γ), and external parameters set by the environment (e.g. resource encounter rate, α). Understanding how marginal changes in one or more of these parameters will affect ξ can provide some intuition about how colonies might adjust it collective behavior to improve robustness to foraging interruptions. We used sensitivity analysis to quantify these relationships [40]. In particular, we employed the normalized forward sensitivity index:

$$\Gamma_\rho^{\mathbf{u}} := \lim_{\delta\rho \to 0} \frac{\left(\frac{\delta \mathbf{u}}{\mathbf{u}} \right)}{\left(\frac{\delta \rho}{\rho} \right)} = \frac{\rho}{\mathbf{u}} \frac{\partial \mathbf{u}}{\partial \rho} \qquad \mathbf{u} \neq 0 \tag{15}$$

where $\mathbf{u}$ defines the output measurement and ρ is a nominal input parameter [40]. For our purposes, the normalized sensitivity index ($\Gamma_\rho^{\mathbf{u}}$) is a dimensionless number that effectively estimates the expected percent change of a relevant metric (e.g. $\mathcal{R}_0$) given a unit percentage change (i.e. $\pm 1\%$) of a model parameter.

From equations (14) and (15) it is straightforward to calculate expressions defining $\Gamma_\rho^{\mathcal{R}_0}$ and $\Gamma_\rho^{\mathcal{R}_\Delta}$ as a function of model parameters. Table 4 lists the predicted indices based on the baseline values given in Table (1). In general, parameters that increase $\mathcal{R}_0$ tended to decrease $\mathcal{R}_\Delta$ (although not always proportionally). For instance, the sensitivity index: $\Gamma_\beta^{\mathcal{R}_0} = +9.5$ tells us that a 1 % increase in the effective contact rate, β should increase $\mathcal{R}_0$ by 9.5% and vice versa (Table 4).

Based on the results, we predict that changes in the effective contact rate (β) should have the largest positive impact on ξ. On the other hand, changes in the death rates of returning foragers (d_f) should have the largest negative impact on ξ, followed by the per-capita forager return rate (γ).

One interesting advantage of the normalized sensitivity index is its usefulness as a tool for doing cost-benefit analysis [40]. Colonies face many kinds of tradeoffs in regulating foraging activity. One such example might be the tradeoff of increasing worker availability (e.g. by increasing the baseline number of available foragers, A_0^*) at a cost of decreasing forager interaction rate due to size limitations of the vestibule (i.e. crowding effects) among others. Assuming these costs can be estimated, $\Gamma_\rho^{\mathbf{u}}$ could be used to define a cost-benefit ratio which may provide some further insights into the regulatory importance of the colony-specific parameters in our model.

4. Numerical Simulations

Previous studies by, [19, 21, 33] among others indicate that colonies of the seed harvester ant *Pogonomyrmex barbatus* may use successful forager return rates to regulate overall foraging activity via worker interactions. Our theoretical results predict that $\mathcal{R}_0$, and $\mathcal{R}_\Delta$ should play an important regulatory roles in

Parameter	Sensitivity Index (Γ^u_ρ)		
	$\mathcal{R}_0$	$\mathcal{R}_\Delta$	ξ
α	$+0.001$	-0.000	$+0.001$
β	$+9.51$	-0.000	$+9.51$
γ	-9.06	$+0.004$	-9.056
k_1	$+0.95$	-0.02	$+0.97$
k_2	-0.95	-0.000	-0.95
d_f	-0.19	$+0.08$	-0.27
d_r	-9.06	$+3.92$	-12.9

Table 4: Normalized sensitivity indices (Γ^u_ρ) of the robustness metrics ξ shown for baseline parameter values given in Table 1. Indicies effectively quantify the ratio of changes in the forager recruitment metrics (i.e. $\mathcal{R}_0$, $\mathcal{R}_\Delta$) with respect to perturbations of model parameters.

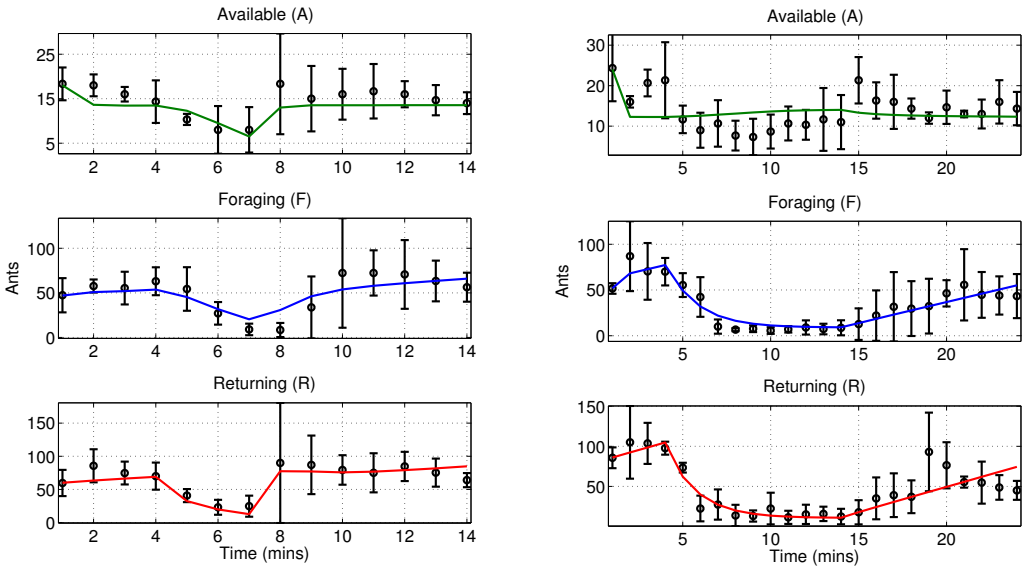

(a) 3 minute removal

(b) 10 minute removal

Figure 5: Simulations of forager removal perturbation experiment described in Pinter-Wollman et al. (2013). Model (4) was fitted (bolded lines) to averaged time-series (circles) of available (top) , foraging (middle), and returning (bottom) foragers for colony N7. Error-bars show the variances between 3 trials reported in Pinter-Wollman et al. Removals began at $t = 4$ and lasted either 3 minutes (left panels) or 10 minutes (right panels). Parameter estimates are given in Table 5

the colony's foraging activities. In this section, we will begin with an empirical validation of model (4) by performing a model fit to experimental data. In addition, we explore a dynamic sensitivity analysis of (4) to identify parameters (in different bifurcation regions) that drive model dynamics, and quantify their effects at both equilibrium (un-disturbed) and perturbed foraging states.

4.1. Model Validation

To examine whether our model simulated realistic response to perturbations, we replicate *in silico* the experimental perturbation described in [19]. In multiple observations over a 3-day period, returning foragers of four mature P. *barbatus* (colonies: N1, N4, N5, & N7) were artificially prevented from entering the nest for either 3 or 10 minutes during periods of high foraging activity. Throughout the trial, the

	Estimated Values			
Parameter	3-min removal	SD	10-min removal	SD
α	.6354	.3930	8.251	15.325
β	.0386	.0236	.5003	0.8878
γ	.4568	.2973	6.028	11.493
k_1	11.067	12.783	10.763	6.532
k_2	34.642	57.712	1.729	6.056

Table 5: Estimated parameters (scaled in minutes) and one-standard deviations for colony N7. Estimates were generated using the Nonlinear grey-box modeling toolbox provided in MATLAB®. Death rates were fixed prior and after the perturbation ($d_f = d_r = 0,\ t < 4, t > 14$) and estimated for returning foragers for 3-minute removals: (a) $d_r = 1.01101 \pm 0.39937,\ t \in [4, 7]$; and 10-minute removals (b) $d_r = 1.01085 \pm 0.278261,\ t \in [4, 14]$. Sampling intervals are same as in Table 1.

numbers of available foragers in the vestibule along with the numbers of outgoing and returning foragers on the trail were recorded. In most instances, the number of outgoing foragers declined in response to the removals and recovered to varying levels of activity once returning foragers were allowed to return to the nest.

To estimate model parameters we used the averaged time-series for each colony (see Table 5 for an example for colony N7). Along with fixed experimental parameters (e.g. times of removal) we generated best-fit response curves corresponding to observations for both 3 and 10 minute removals. Because the quality of fits did not vary extensively among colonies, we show results for one representative colony (N7) (Fig. 5).

Our estimates of $\mathcal{R}_0$ and $\mathcal{R}_\Delta$ after the perturbation indicate that foraging activity was in the bi-stability region during the 3 minute removals ($\mathcal{R}_0 = .03$, $\mathcal{R}_\Delta = .00$) and 10 minute removal ($\mathcal{R}_0 = .52$, $\mathcal{R}_\Delta = .00$). We found similar values in the bi-stability region for colonies N1 and N4 (not shown). These results are consistent with empirical observations noting that colonies will suppress and ultimately suspend foraging activity under sustained perturbations of forager return rates [4]. Our estimates predict a low value of ξ during the recovery phase of the 3 minute removal (i.e. $\xi = .03$) and highlights a limitation of the metric. Short-term disruptions generally elicit small reductions in foraging activity which may have biased our estimates of $\mathcal{R}_0$ too low. Ideally, we would have preferred to generate model fits to the equilibrium foraging activity levels prior to the perturbations, but we did not have sufficient data points.

Finally, we acknowledge some model limitations may have affected the goodness of fit. Most obviously, we do not account for spatial constraints of vestibule size and structure which may influence the baseline numbers of available foragers, interaction patterns inside the vestibule and any delay components affecting the arrival rate of available foragers at the vestibule. Indeed, a summary analysis of the Pinter-Wollman *et al.* (2013) activity data revealed a lagged correlation between the numbers of ants in the vestibule and number of returning foragers (Pearson's product-moment correlation, t = 1.9592, df = 13, p= 0.07189). Such delays should be accounted for in future models.

4.2. Sensitivity Analysis

It is often the case in non-linear systems that the relative importance of one or more parameters on the model dynamics may change in different parameter regions. For our foraging model (4), we are interested in quantifying the effects of important parameters like the colony-specific forager retirement rate (k_2), and determining whether/how these effects may change over time. Understanding these sensitivities can help identify relevant components of robustness in our model.

Mathematically, the sensitivity analysis is done by solving a set of adjoining forward sensitivity equations derived by taking the partial derivatives of (4) with respect to focal parameters (see [40] for a review).

We employed the ODE15s SENS_SYS extension in MATLAB written by V.M. Garcia Molla which calculates and integrates the sensitivity equations in addition to model (4). The output is a time-series of model sensitivities which we normalized to produce indices functionally identical to those described in equation (15).

We initialized system (4) at a positive foraging equilibrium with parameters in the: (a) Persistent activity region ($\mathcal{R}_0 > 1$), and (b) Bistability region ($\max\{\frac{k_1\beta}{k_2(k_1+\gamma)}, \mathcal{R}_\Delta\} < \mathcal{R}_0 < 1$). We then introduce a constant perturbation by increasing the returning forager death rate by 2000% (similar to the experimental perturbation) i.e, $d_r = 0.05,\ t < 20;\ d_r = 1,\ t \in [20, 40]$:

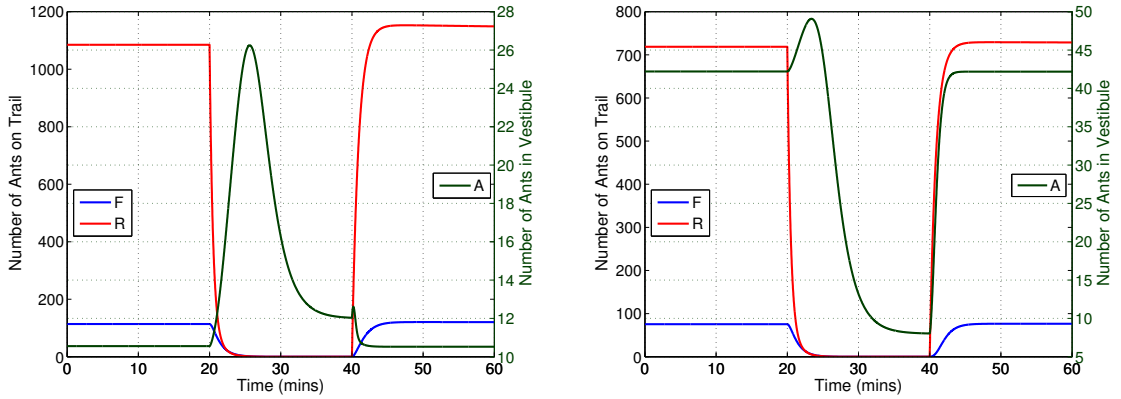

(a) Persistent foraging activity ($\mathcal{R}_0 > 1$)

(b) Bistablity ($\mathcal{R}_\Delta < \mathcal{R}_0 < 1$; $\mathcal{R}_0 > \frac{k_1\beta}{k_2(k_1+\gamma)}$)

Figure 6: Dynamics of system (4) under perturbation. A perturbation is introduced at $t = 20$ by increasing returning forager death rate, d_r by 2000% (red). The number of available foragers (green) increases initially as forager activations declines (blue). The model is initialized at equilibrium with parameters satisfying (a) $\mathcal{R}_0 = .19$, $\mathcal{R}_\Delta = .01$ (b) $\mathcal{R}_0 = 1.19$.

Figures 6(b) and 6(a) show the effects of forager removal on model dynamics. As the perturbation increases beyond $t = 20$, the number of available workers in the vestibule rises initially due to insufficient contacts with returning foragers. However, as we continue to prevent foragers from returning, forager retirement rates ultimately overtake arrival rates at the vestibule, reducing the pool of available foragers. This happens at around $t = 25$. Finally, at $t = 40$, all numbers increase as foragers are allowed to return to the nest, and the system tends back towards equilibrium. In general, the model tends to equilibrate worker availability faster than empirically observed. This difference between model and experiments is largely due to the model assumptions that there is no direct recruitment mechanism from the inner nest to the vestibule (i.e. worker arrivals are independent of forager return rates) and that there are no inherent delays in this dynamic.

There are major differences between the system's response during and after the perturbation period, depending on the parameter region. In the persistent region, i.e., $\mathcal{R}_0 > 1$, the average number of workers in the vestibule in the absence of foraging is relatively higher than it is when there is activity. On the other hand, for the bi-stable region, i.e., $\max\{\frac{k_1\beta}{k_2(k_1+\gamma)}, \mathcal{R}_\Delta\} < \mathcal{R}_0 < 1$, worker availability in the absence of foraging is much lower than it is when forager return rate is positive (Fig. 6). At first glance, this result is counter-intuitive because one might expect persistent foraging activity should be associated with larger numbers of available workers. However, because successful forager return rate is a non-decreasing function of the *forager generation number*, $\mathcal{R}_0$ (and $\mathcal{R}_0$ is an increasing function of the effective contact rate, β) (see Table 4), we may infer that the equilibrium number of available foragers should be relatively lower in the persistent region due to the increased rate of forager recruitment that is the result of a high interaction rate.

Figure 7 a-d shows the corresponding model sensitivities for select parameters as a function of time.

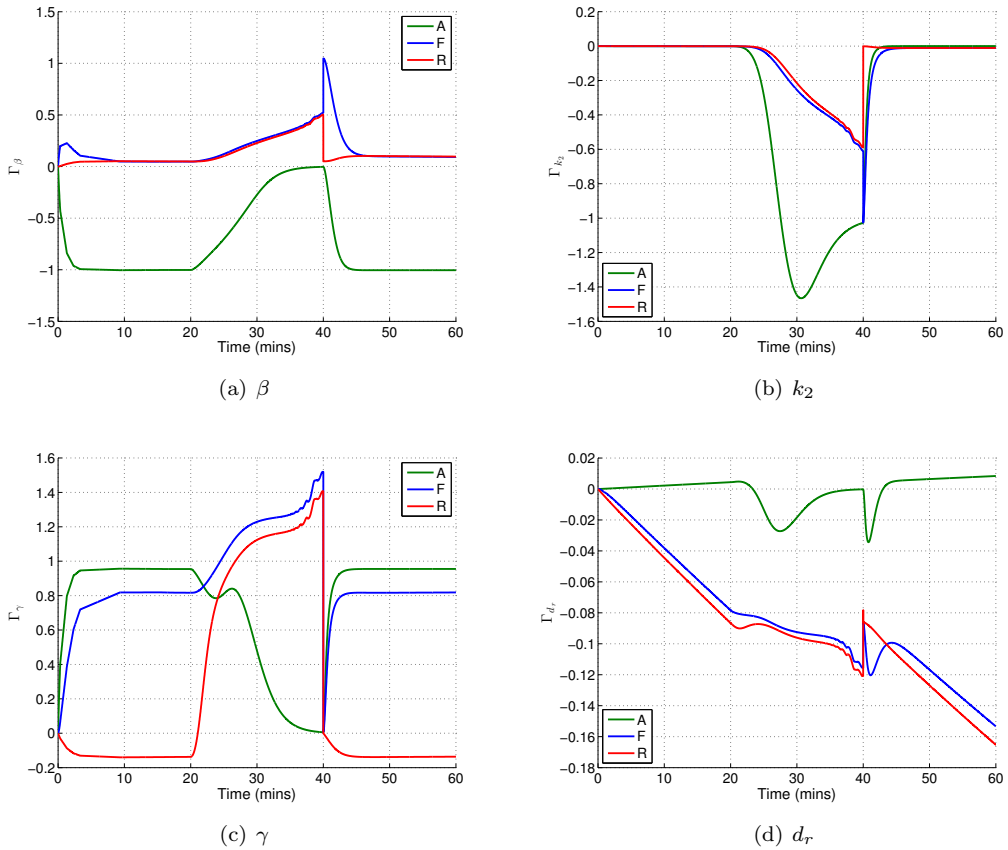

(a) β (b) k_2

(c) γ (d) d_r

Figure 7: Dynamic population sensitivity w.r.t. select model parameters: (a) Effective contact rate, β; (b) Retirement rate, k_2; (c) Forager return rate, γ; (d) Forager death rate, d_r. The model is initialized at equilibrium with $.01 = \mathcal{R}_\Delta < \mathcal{R}_0 = .19 < 1$ (right panel). The sensitivity indices (y-axis) describe the expected percentage change in the numbers of available foragers (green), activated foragers (blue) or returning foragers (red) given an 1% increase in the focal parameter (see equation (15)).

The normalized sensitivity indices (y-axes) describe the expected percentage change in the numbers of available foragers (green), activated foragers (blue) or returning foragers (red) given a 1% increase in the focal parameter (see equation (15) and [40] for a review). Our results show varying patterns of sensitivity for each parameter, and are summarized as follows:

1. Figure 7(a) shows that at equilibrium (i.e. $t < 20$), increasing the effective contact rate (β) should have a negative impact on available foragers (i.e. $\approx 1\%$ reduction) and a small but positive impact on both active and returning foragers. However, as the perturbation unfolds (i.e. $t > 20$), its expected impact on both active and returning foragers increases steadily and peaks near the end of the perturbation period as the numbers of available foragers begin to increase. As discussed previously, the initial increase in the number of ants in the vestibule results from a reduction in forager activation rates. However, the pattern in figure 7(a) tells us that interaction rates are particularly important especially during a perturbation when there are fewer numbers of returning and available foragers.

2. Figure 7(b) shows the effects of increasing forager retirement rate (k_2) at equilibrium is almost negligible in all compartments. However, as the perturbation unfolds, all three compartments show increasing negative sensitivity to k_2 with its largest impact on available foragers. Interestingly, the peak sensitivity for available foragers occurred well before the end of the perturbation (around $t = 30$) as the model

equilibrated around the non-foraging equilibrium. Biologically, this tells us that altering the retirement rate should have minor impacts on foraging intensity once a colony has achieved a steady-state activity level.

3. Figure 7(c) shows the effects of the per-capita forager return rate (γ). At equilibrium, γ should have a large positive impact on available and activated forager numbers. However, as the perturbation unfolds, its predicted impact is largest and positive for both activated and returning foragers. Biologically, we expect that although γ will be influenced by external variables (e.g. average foraging trip length, humidity etc.), colonies that can regulate interaction rates, perhaps by increasing the latency of returning foragers in the vestibule through architectural features, can better manage the impact of fluctuations in forager return rates on the *forager generation number*.

4. Figure 7(d) shows, unsurprisingly, that increasing forager death rates (d_r) should have a consistent negative impact on both active and returning foragers relative to available foragers. Although the magnitude of these effects are small (owing to our parameterization, Table 1) we find that the number of available foragers is least sensitive to d_r at equilibrium but increasingly sensitive whenever A increases.

5. Discussion

We have developed a simple model describing the dynamics of collective foraging activity and regulation with non-spatial forager recruitment with an application to the foraging activities of seed harvester ant colonies. Our modeling approach relies on previous experimental observations that interactions between available and returning foragers may be used to communicate changes in resource abundance and/or environmental conditions outside the nest [4, 19, 21, 23]. Our main result is that depending on model parameters foraging activity may either persist at high levels or may evolve toward one of two co-existing attractors corresponding to an intermediate foraging or non-foraging activity state. The dynamics of our model (4) can be summarized as follows:

- Foraging activity is always persistent when the *forager generation number* ($\mathcal{R}_0 = \frac{k_1}{k_2 A_f^*}$) is greater than one.
- When this fails, but the inequalities $\max\{\frac{k_1\beta}{k_2(k_1+\gamma)}, \mathcal{R}_\Delta\} < \mathcal{R}_0 < 1$ hold, the colony may sustain its foraging activity if the forager generation number is larger than the ratio between the rate of new worker arrivals at the vestibule (from inside the nest) and the maximum forager return rate (i.e. $\mathcal{R}_0 > \mathcal{R}_\Delta = \frac{k_1}{\phi_{\max}}$).

Previous modeling studies have assumed that returning foragers have a constant effect on the rate of forager recruitment without identifying any underlying causal parameters [29, 32]. Here, we defined the forager generation number ($\mathcal{R}_0$) as the average number of recruits per returning forager over the typical duration of a foraging trip. Foraging activity is self-sustaining and most robust to perturbations as long as each returning forager generates sufficient contacts to recruit at least one available forager ($\mathcal{R}_0 > 1$). Declines in forager returns or changes in worker availability due to decreasing worker arrival rates (or increasing retirement rates) can decrease forager generation number. If $\mathcal{R}_0$ is less than one, but larger than a threshold value ($\mathcal{R}_\Delta$), then foraging activity exists in a region of bistability as long as the equilibrium rate at which foragers become available is larger than the rates at which they become activated (i.e. $\max\{\frac{k_1\beta}{k_2(k_1+\gamma)}, \mathcal{R}_\Delta\} < \mathcal{R}_0 < 1$). Our simulations show that the size of this region: $\xi = \mathcal{R}_0 - \mathcal{R}_\Delta$, is negatively correlated with the basin of attraction for the non-foraging equilibrium (Fig. 4). In some sense, ξ provides an indication of how small the colony's workforce can be in order to sustain its foraging activity. Thus, we suggest that colonies with larger values of ξ may be better able to sustain foraging activity during periods of low forager return (e.g. due to predation on the trail) compared with colonies with smaller vales of ξ.

A sensitivity analysis of $\mathcal{R}_0$ indicated that it is most positively impacted by the effective contact rate, β, and to a lesser extent by the rate of worker arrivals and forager retirement, k_1 & k_2 respectively (Table

4). On the other hand, an increase in per-capita returning forager death rate, d_r, had the largest negative impact on $\mathcal{R}_0$, followed by the per-capita forager return rate, γ (Table 4). These results suggest that the management of interaction rates inside the vestibule and the adjustment of latency periods within the nest (i.e., for returning foragers) are important components likely to have the greatest impact on the regulation of a colony's foraging activity.

Simulated perturbations of our model revealed qualitatively similar dynamics to those observed in empirical studies. Short periods of forager removal were followed by a quick recovery of prior activity levels, but long removal periods were followed by slower recovery (Fig. 5). The observed patterns of recovery were fairly consistent with the data despite the model not accounting for explicit information delays (e.g. travel time from the food source, arrival from the inner nest at the vestibule, etc.). Our estimates of the forager generation number for the colonies sampled by Pinter-Wollman *et al.* [19] fell within the bi-stable region ($\max\{\frac{k_1\beta}{k_2(k_1+\gamma)}, \mathcal{R}_\Delta\} < \mathcal{R}_0 < 1$). This finding is consistent with previous work showing that colonies temporarily suspended foraging under sustained disruptions of forager return rates [4]. Moreover, our colony estimates of ξ and patterns of recovery after the perturbation varied among colonies, suggesting that there are potential colony-specific differences in the robustness of their foraging activities [29].

Our model also makes testable predictions about the expected number of available workers in the vestibule as a function of foraging intensity: (1) colonies with a forager generation number larger than one are likely to have a greater baseline number of available workers during periods of low foraging returns and comparatively lower numbers during periods of high forager returns, and (2) colonies with a forager generation number less than one are likely to have greater numbers of available foragers during periods of high returns and lower numbers as forger return rates decline.

Our analysis indicates that the dynamics of forager availability in the vestibule may play a particularly important role in sustaining activity when forager return rates are low. The vestibule must be populated sparsely, not densely, in order to keep forager activation rates high. Because an individual worker's retirement decision is made based on her perception of local forager densities inside the vestibule, colonies may differ in their level of responsiveness to forager return rates simply based on worker response thresholds. Pinter-Wollman *et al.* [19] reported inter-colony variation in the differences between per-capita interaction rates (within the vestibule) at high versus low forger return periods. Furthermore, Gordon [29] found variable effects of outside humidity on forager activation rates among colonies. Intuitively, one might expect that colonies containing foragers that respond uniformly to reductions in return rates (by retiring from the vestibule) may be less robust to short-term foraging interruptions compared to colonies with more diverse worker thresholds [41].

An important biological insight of our results is that an interaction-based forager recruitment strategy shares many of the regulatory strengths of leader-based recruitment (e.g. tandem running), and self-organizing chemical recruitment (e.g. pheromone trails). Although tandem running conveys more direct information about foraging conditions, which can allow the colony to flexibly respond to short-term changes in environmental profitability, it critically lacks the mass-recruitment properties of self-reinforcing pheromone trail networks[11]. On the other hand, the strong reinforcing feedbacks that associate trail quality with forager usage and pheromone strength can often weaken the colony's ability to flexibly track changes in resource quality [16]. Moreover, the fidelity of pheromone-based trail networks is often limited by volatility and degradation under variable environmental conditions outside the control of the colony. The interaction-based recruitment modeled strategy circumvents these limitations because it is both self-organizing (because every returning forager is a potential recruiter), and can be more readily/directly controlled by the colony (e.g. by adjusting forager availability and interaction patterns in response to fluctuations in forager return rates).

In conclusion, our results support growing evidence that a simple interaction-based forager recruitment can provide a robust regulatory system for collective foraging in ant colonies [19, 23]. Furthermore, they provide clear intuitions behind the mechanisms and parameters likely to influence collective foraging dynamics, and identify potential sources of observed inter-colony variability in responsiveness and activity patterns under experimental conditions [29]. Our current model, however, does not include some potentially important regulatory components that have been identified empirically [19]. Two such examples include the influence of multiple time scales and information delays on foraging regulation, as well as the effects of spatial constraints on interaction patterns inside the vestibule. We will incorporate these complexities into our model in our future work.

6. Proofs

Proof of Theorem 3.1

Proof. According to the formulation of the foraging model (4), the following holds for $(A, F, R) \in \mathbb{R}^3_+$:

$$\begin{aligned} A'|_{A=0} &= k_1 + \gamma R \geq k_1 \\ F'|_{F=0} &= \beta AR \geq 0 \\ R'|_{R=0} &= \alpha F \geq 0. \end{aligned}$$

Thus, applying the results of Theorem A.4, p.423 in Thieme (2003), we can conclude that the foraging model (4) is positively invariant in $\mathbb{R}^3_+$.

Let $N = A + F + R$, then we have

$$N' = A' + F' + R' = k_1 - \tfrac{k_2 A}{1+R} - d_f F - d_r R.$$

Thus, we have the following inequalities based on the property of the positivity invariance:

$$k_1 - \max\{k_2, d_f, d_r\}N \leq k_1 - k_2 A - d_f F - d_r R \leq N' \leq \frac{k_1(1+R) - k_2 A - d_f F - d_r R(1+R)}{1+R}.$$

This indicates the following two cases:

1. **Bounded below:**

$$N' \geq k_1 - \max\{k_2, d_f, d_r\}N \Rightarrow \liminf_{t\to\infty} N(t) \geq \tfrac{k_1}{\max\{k_2, d_f, d_r\}}.$$

2. **Bounded above:**

$$\begin{aligned} N' &\leq \tfrac{k_1(1+R) - k_2 A - d_f F - d_r R(1+R)}{1+R} = \tfrac{k_1(1+R) - d_r R^2 - k_2 A - d_f F - d_r R}{1+R} \\ &\leq \tfrac{k_1(1+R) - d_r R^2 - \min\{k_2, d_f, d_r\}N}{1+R} = \tfrac{-d_r\left(R - \frac{k_1}{2d_r}\right)^2 + \frac{k_1^2}{4d_r} + k_1 - \min\{k_2, d_f, d_r\}N}{1+R} \\ &\leq \tfrac{\frac{k_1^2}{4d_r} + k_1 - \min\{k_2, d_f, d_r\}N}{1+R}. \end{aligned}$$

This indicates that

$$\limsup_{t\to\infty} N(t) \leq \frac{k_1 + \frac{k_1^2}{4d_r}}{\min\{k_2, d_f, d_r\}}.$$

Therefore, we can conclude that every trajectory starting in $\mathbb{R}^3_+$ is attracted to the following compact set

$$C = \left\{ (A,F,R) \in \mathbb{R}^3_+ : \frac{k_1}{\max\{k_2, d_f, d_r\}} \leq A + F + R \leq \frac{k_1 + \frac{k_1^2}{4d_r}}{\min\{k_2, d_f, d_r\}} \right\}$$

which also implies that the foraging dynamics of Model (4) can be restricted to the compact set C.

Let $M = \frac{k_1 + \frac{k_1^2}{4d_r}}{\min\{k_2, d_f, d_r\}}$. Because Model (4) is bounded by M, the number of returning ants R is also bounded by M. This implies that for any $\epsilon > 0$, there exists time T large enough, such that we have

$$A' = k_1 - \beta AR + \gamma R - k_2 \frac{A}{1+R} \geq k_1 - \beta(M+\epsilon)A - k_2 A \geq k_1 - (\beta(M+\epsilon) + k_2)\, A, \text{ for all } t > T.$$

This indicates that

$$\liminf_{t\to\infty} A(t) \geq \frac{k_1}{\beta M + k_2}.$$

Therefore, we can conclude that A is persistent in $\mathbb{R}^3_+$. □

Proof of Theorem 3.2

Proof. Because the **non-foraging equilibrium** $\mathscr{E}_{\mathbf{0}} = (A_0^*, 0, 0) = (\frac{k_1}{k_2}, 0, 0)$ always exists, we focus on sufficient conditions lead to the existence of the **foraging equilibrium** $\mathscr{E}_{\mathbf{i}} = (A_f^*, F_i^*, R_i^*) = \left(A_f^*, \frac{\gamma+d_r}{\alpha} R_i^*, R_i^*\right), i = 1, 2$ where $A_f^* = \frac{(\alpha+d_f)(\gamma+d_r)}{\alpha\beta}$ and R_i^* are roots of the equation $\phi(R^*) = k_2 A_f^*$ with

$$\phi(R) = \left[k_1 - (\beta A_f^* - \gamma)R\right](1+R).$$

Therefore, the existence of $\mathscr{E}_{\mathbf{i}}$ is determined by the positive intercept(s) of the quadratic function $\phi(R)$ and the horizontal line $k_2 A_f^*$, which can be classified into the following two cases depending on the sign of the critical point $R_c = \frac{\gamma - \beta A_f^* + k_1}{2(\beta A_f^* - \gamma)}$ of $\phi(R)$ (see Fig. 2(b)):

1. If $R_c < 0$ (see Fig. 2(a)), then we have

$$R_c = \frac{\gamma - \beta A_f^* + k_1}{2(\beta A_f^* - \gamma)} < 0 \Leftrightarrow A_f^* > \frac{k_1 + \gamma}{\beta} \Leftrightarrow k_1 < d_r + \frac{d_f(\gamma + d_r)}{\alpha} \Leftrightarrow \mathcal{R}_0 = \frac{k_1}{k_2 A_f^*} < \frac{k_1 \beta}{k_2(k_1 + \gamma)}.$$

   In this case, the foraging dynamics can have $\mathscr{E}_{\mathbf{0}}$ or $\mathscr{E}_{\mathbf{i}}, i = 0, 2$ depending on the ratio of $\frac{\phi(0)}{k_2 A_f^*} = \frac{k_1}{k_2 A_f^*}$:

   (a) If $\frac{\phi(0)}{k_2 A_f^*} = \frac{k_1}{k_2 A_f^*} < 1$ (i.e., $\mathcal{R}_0 < 1$, see the purple horizontal line in Fig. 2(a)), then either there is no intercept of the null clines or the intercepts of $\phi(R)$ and the horizontal line $k_2 A_f^*$ are located in the black region (i.e., negative values). In this scenario, the foraging model (4) only has the **non-foraging equilibrium** $\mathscr{E}_{\mathbf{0}}$.

   (b) If $\frac{\phi(0)}{k_2 A_f^*} = \frac{k_1}{k_2 A_f^*} > 1$ (i.e., $\mathcal{R}_0 > 1$, see the cyan horizontal line in Fig. 2(a)), then there is a unique foraging equilibrium $\mathscr{E}_{\mathbf{2}}$. Thus, in this scenario, the foraging model (4) has the **non-foraging equilibrium** $\mathscr{E}_{\mathbf{0}}$ and the **foraging equilibrium** $\mathscr{E}_{\mathbf{2}}$.

2. If $R_c > 0$ (see Fig. 2(b)), then we have

$$R_c = \frac{\gamma - \beta A_f^* + k_1}{2(\beta A_f^* - \gamma)} < 0 \Leftrightarrow A_f^* < \frac{k_1 + \gamma}{\beta} \Leftrightarrow k_1 > d_r + \frac{d_f(\gamma + d_r)}{\alpha} \Leftrightarrow \mathcal{R}_0 = \frac{k_1}{k_2 A_f^*} > \frac{k_1 \beta}{k_2(k_1 + \gamma)}.$$

In this case, the foraging dynamics can have $\mathscr{E}_{\mathbf{0}}$ or $\mathscr{E}_{\mathbf{i}}, i = 0, 2$ or $\mathscr{E}_{\mathbf{i}}, i = 0, 1, 2$ depending on the ratio of $\frac{\phi(0)}{k_2 A_f^*} = \frac{k_1}{k_2 A_f^*}$ and $\frac{\phi_{max}}{k_2 A_f^*}$:

(a) If $k_2 A_f^* > \phi_{max} \geq \phi(0) = k_1$, we have

$$k_2 A_f^* > \phi_{max} \geq \phi(0) = k_1 \Leftrightarrow 0 < \mathcal{R}_0 = \frac{k_1}{k_2 A_f^*} < \mathcal{R}_\Delta = \frac{k_1}{\phi_{max}}.$$

In this case, the horizontal line $k_2 A_f^*$ (see the purple horizontal line in Fig. 2(b)) is above the quadratic equation $\phi(R)$, i.e., there is no foraging equilibrium. Thus, in this scenario, the foraging model (4) has only the **non-foraging equilibrium** $\mathscr{E}_{\mathbf{0}}$.

(b) If $k_1 < k_2 A_f^* < \phi_{max}$ (see the dark green horizontal line in Fig. 2(b)), then we have the following equalities:

$$k_1 < k_2 A_f^* < \phi_{max} \Leftrightarrow 0 < \mathcal{R}_\Delta = \frac{k_1}{\phi_{max}} < \frac{k_1}{k_2 A_f^*} = \mathcal{R}_0 < 1 < \frac{k_2 A_f^*}{\phi_{max}}.$$

In this scenario, the foraging model (4) has the **non-foraging equilibrium** $\mathscr{E}_{\mathbf{0}}$ and two **foraging equilibria** $\mathscr{E}_{\mathbf{i}}, i = 1, 2$.

(c) If $\frac{\phi(0)}{k_2 A_f^*} = \frac{k_1}{k_2 A_f^*} > 1$ (i.e., $\mathcal{R}_0 > 1$, see the cyan horizontal line in Fig. 2(b)), then there is a unique foraging equilibrium $\mathscr{E}_{\mathbf{2}}$. Thus, in this scenario, the foraging model (4) has the **non-foraging equilibrium** $\mathscr{E}_{\mathbf{0}}$ and the **foraging equilibrium** $\mathscr{E}_{\mathbf{2}}$.

Now we focus on the local stability of the **non-foraging equilibrium** $\mathscr{E}_{\mathbf{0}}$ and two **foraging equilibria** $\mathscr{E}_{\mathbf{i}}, i = 1, 2$ when they exist. According to the Jacobian matrix (13) evaluated at an equilibrium, we know that the local stability of $\mathscr{E}_{\mathbf{0}}$ is determined by the eigenvalues $\lambda_i, i = 1, 2, 3$ of the following Jacobian matrix

$$J|_{\mathscr{E}_{\mathbf{0}}} := \begin{bmatrix} -k_2 & 0 & -\frac{\beta k_1}{k_2} + k_1 + \gamma \\ 0 & -(\alpha + d_f) & \frac{\beta k_1}{k_2} \\ 0 & \alpha & -(\gamma + d_r) \end{bmatrix}$$

where

$$\lambda_1 = -k_2,\ \lambda_2 + \lambda_3 = -(\alpha + d_f + d_r + \gamma) < 0, \text{ and } \lambda_2 \lambda_3 = \frac{-\alpha\beta k_1}{k_2} + (\gamma + d_r)(\alpha + d_f) = (\gamma + d_r)(\alpha + d_f)\left[1 - \mathcal{R}_0\right].$$

This indicates that if $\mathcal{R}_0 < 1$, then $\lambda_i < 0, i = 1, 2, 3$; while if $\mathcal{R}_0 > 1$, then $\lambda_i > 0, 2, 3$. Therefore, $\mathscr{E}_{\mathbf{0}}$ is locally asymptotically stable if $\mathcal{R}_0 < 1$ and it is a saddle if $\mathcal{R}_0 > 1$.

The Jacobian matrix evaluate at $\mathscr{E}_i, i = 1, 2$ can be represented as follows:

$$J|_{\mathscr{E}_i} := \begin{bmatrix} -\beta R_i^* - \frac{k_2}{1 + R_i^*} & 0 & -\beta A_f^* + \gamma + \frac{k_2 A_f^*}{(1 + R_i^*)^2} \\ \beta R_i^* & -(\alpha + d_f) & \beta A_f^* \\ 0 & \alpha & -(\gamma + d_r) \end{bmatrix}$$

whose eigenvalues satisfy the characteristic polynomial:

$$\rho(\lambda) = \lambda^3 + c_2 \lambda^2 + c_1 \lambda + c_0 = 0 \tag{16}$$

with

$$
\begin{aligned}
c_2 &= \beta R_i^* + (\alpha + d_f + d_r + \gamma) + \frac{k_2}{1+R_i^*} > 0 \\
c_1 &= (\alpha + d_f + d_r + \gamma)\left[\beta R_i^* + \frac{k_2}{1+R_i^*}\right] > 0 \\
c_0 &= \beta R_i^* \left[(\gamma + d_r)d_f + \alpha d_r\right] - \frac{k_2 R_i^* (\gamma + d_r)(\alpha + d_f)}{(1+R_i^*)^2}
\end{aligned}
\tag{17}
$$

According to the Routh-Hurwitz criteria [42], we can conclude that the **foraging equilibrium** $\mathscr{E}_{\mathbf{i}}$ is locally asymptotically stable if and only if $c_1 c_2 > c_0 > 0$. According to (17), we have

1. $c_1 c_2 > \beta R_i^* (\alpha + d_f + d_r + \gamma)^2$ indicates that

$$
c_1 c_2 - c_0 > \beta R_i^* (\alpha + d_f + d_r + \gamma)^2 - \beta R_i^* \left[(\gamma + d_r)d_f + \alpha d_r\right] > 0.
$$

   Because $c_1 c_2 > c_0 \Leftrightarrow c_1 c_2 - c_0 > 0$, thus, we can conclude $c_1 c_2 > c_0$ always holds for both $R_i^*, i = 1, 2$.

2. The following equivalent relationships holds

$$
\begin{aligned}
c_0 > 0 \Leftrightarrow \quad & \beta(1+R_i^*)^2 \left[(\gamma + d_r)d_f + \alpha d_r\right] - k_2(\gamma + d_r)(\alpha + d_f) > 0 \\
\Leftrightarrow \quad & (1+R_i^*)^2 > \frac{k_2(\gamma + d_r)(\alpha + d_f)}{\beta\left[(\gamma + d_r)d_f + \alpha d_r\right]} = \frac{k_2 A_f^*}{\beta A_f^* - \gamma}
\end{aligned}
\tag{18}
$$

   Notice that $0 < R_1^* < R_2^*$ are roots of $\phi(R) = k_2 A_f^*$, thus we have

$$
\phi(R_i^*) = \left[k_1 - (\beta A_f^* - \gamma)R_i^*\right](1 + R_i^*) = k_2 A_f^* \Leftrightarrow \left[\frac{k_1}{\beta A_f^* - \gamma} - R_i^*\right](1 + R_i^*) = \frac{k_2 A_f^*}{\beta A_f^* - \gamma}.
$$

   This indicates that

$$
\begin{aligned}
c_0 > 0 \quad &\Leftrightarrow \quad (1+R_i^*)^2 > \left[\tfrac{k_1}{\beta A_f^* - \gamma} - R_i^*\right](1 + R_i^*) \\
&\Leftrightarrow \quad 1 + R_i^* > \tfrac{k_1}{\beta A_f^* - \gamma} - R_i^* \\
&\Leftrightarrow \quad R_i^* > \tfrac{k_1}{2(\beta A_f^* - \gamma)} - \tfrac{1}{2}
\end{aligned}
$$

   Recall that

$$
\begin{aligned}
R_1^* &= \frac{k_1}{2(\beta A_f^* - \gamma)} - \frac{1}{2} - \sqrt{\left(\frac{k_1}{2(\beta A_f^* - \gamma)} - \frac{1}{2}\right)^2 + \frac{k_1 - k_2 A_f^*}{\beta A_f^* - \gamma}} \\
R_2^* &= \frac{k_1}{2(\beta A_f^* - \gamma)} - \frac{1}{2} + \sqrt{\left(\frac{k_1}{2(\beta A_f^* - \gamma)} - \frac{1}{2}\right)^2 + \frac{k_1 - k_2 A_f^*}{\beta A_f^* - \gamma}}
\end{aligned}
\tag{19}
$$

   Then we have

$$
\begin{aligned}
R_1^* \quad &< \quad \tfrac{k_1}{2(\beta A_f^* - \gamma)} - \tfrac{1}{2} \Rightarrow c_0 < 0 \\
R_2^* \quad &> \quad \tfrac{k_1}{2(\beta A_f^* - \gamma)} - \tfrac{1}{2} \Rightarrow c_0 > 0
\end{aligned}
$$

The discussion above implies that if the **foraging equilibrium** $\mathscr{E}_{\mathbf{i}}$ exists, then $\mathscr{E}_{\mathbf{1}}$ is always a saddle and $\mathscr{E}_{\mathbf{2}}$ is always locally asymptotically stable.

□

Proof of Corollary 3.1

Proof. According to Theorem 3.1, every trajectory of the foraging model (4) attracts to a compact set C defined in (5). Thus we can restrict the dynamics of Model (4) in this compact set C. Based on the proof of Theorem 3.2, we have the following three cases:

1. If $\mathcal{R}_0 < \min\{1, \frac{k_1\beta}{k_2(k_1+\gamma)}\}$ or $\frac{k_1\beta}{k_2(k_1+\gamma)} < \mathcal{R}_0 < \mathcal{R}_\Delta$, then the foraging model (4) has only *the non-foraging equilibrium* $\mathscr{E}_{\mathbf{0}} = (\frac{k_1}{k_2}, 0, 0)$ which is locally asymptotically stable. Model (4) enters a compact set C and has a unique locally stable equilibrium $\mathscr{E}_{\mathbf{0}}$. Thus, $\mathscr{E}_{\mathbf{0}}$ is globally stable by applying the results of Poincare-Bendixson trichotomy in three dimensional systems [43].

2. If $\mathcal{R}_0 > 1$, then the foraging model (4) has *the non-foraging equilibrium* $\mathscr{E}_{\mathbf{0}}$ and *the foraging equilibrium* $\mathscr{E}_{\mathbf{2}}$ where $\mathscr{E}_{\mathbf{0}}$ is a saddle and $\mathscr{E}_{\mathbf{2}}$ is locally asymptotically stable. Therefore, by applying the results of Poincare-Bendixson trichotomy in three dimensional systems [43], we can conclude that every trajectory starting with strict positive initial condition converges to $\mathscr{E}_{\mathbf{2}}$, i.e., and $\mathscr{E}_{\mathbf{2}}$ is globally stable.

3. If $\max\{\frac{k_1\beta}{k_2(k_1+\gamma)}, \mathcal{R}_\Delta\} < \mathcal{R}_0 < 1$, then the foraging model (4) has *the non-foraging equilibrium* $\mathscr{E}_{\mathbf{0}}$ and *two foraging equilibria* $\mathscr{E}_{\mathbf{i}}, i = 1, 2$ where both $\mathscr{E}_{\mathbf{0}}$ and $\mathscr{E}_{\mathbf{2}}$ are locally asymptotically stable. This implies that the foraging model (4) has bistability, i.e., depending on the initial condition, the trajectory may converge to *the non-foraging equilibrium* $\mathscr{E}_{\mathbf{0}}$ or the *foraging equilibrium* $\mathscr{E}_{\mathbf{2}}$.

□

Acknowledgements

O.U's research is supported by the Graduate Assistance in Areas of National Need Fellowship (DOE-GAANN) and Mathematical, Computational and Modeling Sciences Center (MCMSC). Y.K's research is partially supported by NSF-DMS (Award Number 1313312), Simons Collaboration Grants for Mathematicians (208902) and the research scholarship from School of Letters and Sciences. NPW was funded by the NIH P50 San Diego Center for Systems Biology (SDCSB) grant #GM085764.

References

[1] Detrain, C., Deneubourg, J. L., & Pasteels, J. M. (1999). Decision-making in foraging by social insects. In Information processing in social insects (pp. 331-354).

[2] Adler, F. R., & Gordon, D. M. (1992). Information collection and spread by networks of patrolling ants. American Naturalist, 373-400.

[3] Beshers, S. N., & Fewell, J. H. (2001). Models of division of labor in social insects. Annual review of entomology, 46(1), 413-440.

[4] Gordon, D. M. (2002). The regulation of foraging activity in red harvester ant colonies. The American Naturalist, 159(5), 509-518.

[5] Fewell, J. H., & Winston, M. L. (1992). Colony state and regulation of pollen foraging in the honey bee, Apis mellifera L. Behavioral Ecology and Sociobiology, 30(6), 387-393.

[6] Bonabeau, E., Theraulaz, G., Deneubourg, J. L., Aron, S., & Camazine, S. (1997). Self-organization in social insects. Trends in Ecology & Evolution, 12(5), 188-193.

[7] Dornhaus, A., & Chittka, L. (2004). Information flow and regulation of foraging activity in bumble bees (Bombus spp.). Apidologie, 35(2), 183-192.

[8] Holldobler B, Wilson EO (1990) The Ants: Belknap Press

[9] Franks NR, & Richardson T (2006) Teaching in tandem-running ants. Nature 439:153.

[10] Fernandez AA, & Deneubourg JL (2011) On following behaviour as mechanism for collective movement. Journal of Theoretical Biology 284: 715.

[11] Traniello, J. F. (1989). Foraging strategies of ants. Annual review of entomology, 34(1), 191-210.

[12] Collignon, B., Louis Deneubourg, J., & Detrain, C. (2012). Leader-based and self-organized communication: Modelling group-mass recruitment in ants. Journal of theoretical biology.

[13] Sumpter, D., & Pratt, S. (2003). A modelling framework for understanding social insect foraging. Behavioral Ecology and Sociobiology, 53(3), 131-144

[14] Deneubourg, J. L., Goss, S., Franks, N., & Pasteels, J. M. (1989). The blind leading the blind: modeling chemically mediated army ant raid patterns. Journal of insect behavior, 2(5), 719-725.

[15] Beekman, M., Sumpter, D. J., & Ratnieks, F. L. (2001). Phase transition between disordered and ordered foraging in Pharaoh's ants. Proceedings of the National Academy of Sciences, 98(17), 9703-9706.

[16] Dussutour, A., & Nicolis, S. C. (2013). Flexibility in collective decision-making by ant colonies: Tracking food across space and time. Chaos, Solitons & Fractals.

[17] Tabone, M., Ermentrout, B., & Doiron, B. (2010). Balancing organization and flexibility in foraging dynamics. Journal of theoretical biology, 266(3), 391-400.

[18] Greene, M. J., & Gordon, D. M. (2007). How patrollers set foraging direction in harvester ants. The American Naturalist, 170(6), 943-948.

[19] Pinter-Wollman, N., Bala, A., Merrell, A., Queirolo, J., Stumpe, M. C., Holmes, S., & Gordon, D. M. (2013). Harvester ants use interactions to regulate forager activation and availability. Animal Behaviour.

[20] Gordon, D. M., Holmes, S., & Nacu, S. (2008). The short-term regulation of foraging in harvester ants. Behavioral Ecology, 19(1), 217-222.

[21] Greene, M. J., & Gordon, D. M. (2007). Interaction rate informs harvester ant task decisions. Behavioral Ecology, 18(2), 451-455.

[22] Gordon, D. M. (2010). Ant encounters: interaction networks and colony behavior. Princeton University Press.

[23] Greene, M. J., Pinter-Wollman, N., & Gordon, D. M. (2013). Interactions with combined chemical cues inform harvester ant foragers' decisions to leave the nest in search of food. PloS one, 8(1), e52219.

[24] Beverly, B. D., McLendon, H., Nacu, S., Holmes, S., & Gordon, D. M. (2009). How site fidelity leads to individual differences in the foraging activity of harvester ants. Behavioral Ecology, 20(3), 633-638.

[25] Gordon, D. M. (1998). Task-related differences in the cuticular hydrocarbon composition of harvester ants, Pogonomyrmex barbatus. Journal of Chemical Ecology, 24(12), 2021-2037.

[26] Wagner, D., Brown, M. J., Broun, P., Cuevas, W., Moses, L. E., Chao, D. L., & Gordon, D. M. (1998). Task-related differences in the cuticular hydrocarbon composition of harvester ants, Pogonomyrmex barbatus. Journal of Chemical Ecology, 24(12), 2021-2037.

[27] Munger, J. C. (1984). Long-term yield from harvester ant colonies: implications for horned lizard foraging strategy. Ecology, 1077-1086.

[28] Pol, R. G., Lopez de Casenave, J., & Pirk, G. I. (2011). Influence of temporal fluctuations in seed abundance on the foraging behaviour of harvester ants (Pogonomyrmex spp.) in the central Monte desert, Argentina. Austral Ecology, 36(3), 320-328.

[29] Gordon, D. M., Dektar, K. N., & Pinter-Wollman, N. (2013). Harvester ant colony variation in foraging activity and response to humidity. PloS one, 8(5), e63363.

[30] Pacala, S. W., Gordon, D. M., & Godfray, H. C. J. (1996). Effects of social group size on information transfer and task allocation. Evolutionary Ecology, 10(2), 127-165.

[31] Nicolis, S. C., Theraulaz, G., & Deneubourg, J. L. (2005). The effect of aggregates on interaction rate in ant colonies. Animal behaviour, 69(3), 535-540.

[32] Prabhakar, B., Dektar, K. N., & Gordon, D. M. (2012). The regulation of ant colony foraging activity without spatial information. PLoS computational biology, 8(8), e1002670.

[33] Schafer, R. J., Holmes, S., & Gordon, D. M. (2006). Forager activation and food availability in harvester ants. Animal Behaviour, 71(4), 815-822.

[34] Gordon, D. M., Guetz, A., Greene, M. J., & Holmes, S. (2011). Colony variation in the collective regulation of foraging by harvester ants. Behavioral Ecology,22(2), 429-435.

[35] Jeanne, R. L. (1986). The organization of work in Polybia occidentalis: costs and benefits of specialization in a social wasp. Behavioral Ecology and Sociobiology, 19(5), 333-341.

[36] Pratt, S. C. (2005). Quorum sensing by encounter rates in the ant Temnothorax albipennis. Behavioral Ecology, 16(2), 488-496.

[37] Gordon, D. M. (1991). Behavioral flexibility and the foraging ecology of seed-eating ants. American Naturalist, 379-411.

[38] Gordon, D. M. (1996). The organization of work in. Nature, 380, 14.

[39] Johnson, R. A. (1991). Learning, memory, and foraging efficiency in two species of desert seed-harvester ants. Ecology, 1408-1419.

[40] Arriola, L., & Hyman, J. M. (2009). Sensitivity analysis for uncertainty quantification in mathematical models. In Mathematical and Statistical Estimation Approaches in Epidemiology (pp. 195-247). Springer Netherlands.

[41] Oldroyd, B. P., & Fewell, J. H. (2007). Genetic diversity promotes homeostasis in insect colonies. Trends in Ecology & Evolution, 22(8), 408-413.

[42] Brauer, F., & Castillo-Chavez, C. (2012). Mathematical models in population biology and epidemiology. Springer.

[43] Thieme, H. R. (1992). Convergence results and a Poincar?-Bendixson trichotomy for asymptotically autonomous differential equations. Journal of mathematical biology, 30(7), 755-763.

[44] Thieme, H. R. (2003). Mathematics in population biology. Princeton University Press.

[45] Smith, H. L., & Thieme, H. R. (2011). Dynamical systems and population persistence (Vol. 118). American Mathematical Soc.